Proposal to the Jefferson Lab PAC-27

Measurement of polarization observables in η-photoproduction with CLAS

J. Ball, P. Collins, M. Dugger*, E. Pasyuk*†, B. G. Ritchie
Arizona State University, Tempe, AZ 85287-1504,
R. A. Arndt, N. Benmouna, B. L. Berman, W. J. Briscoe,
G. Feldman, Y. Y. Ilieva, H. Juengst, P. Nadel-Turonski,
I. I. Strakovsky, S. Strauch, R. L. Workman
The George Washington University, Washington, DC 20052
H. Crannell, F. J. Klein, J. Santoro, D. I. Sober
The Catholic University of America, Washington, DC 20064
D. G. Ireland, J. D. Kelly, K. Livingston, G. Rosner
University of Glasgow, Glasgow G12 8QQ, United Kingdom
C. Djalali, O. Dzyubak, D. Tedeschi
University of South Carolina, Columbia, SC 29208
V. Burkert, V. Mokeev, S. Stepanyan
Thomas Jefferson National Accelerator Facility, Newport News, VA 23606
R. Miskimen, M. Wood
University of Massachusetts, Amherst, MA 01003
V. Crede, P. Eugenio
Florida State University, Tallahassee, FL 32306
P. L. Cole
Idaho State University, Pocatello, ID 83209
D. Jenkins
Virginia Polytechnic Institute and State University, Blacksburg, VA 24061
M. Khandaker
Norfolk State University, Norfolk, VA 23504
M. F. Vineyard
Union College, Schenectady, NY 12308
V. Kouznetsov
Institute for Nuclear Research, 117312, Moscow, Russia

and CLAS Collaboration

December 6, 2004

*co-spokesperson
†contact person, e-mail: pasyuk@jlab.org

Abstract

Among the most exciting and challenging topics in subnuclear physics today is the study of the structure of the nucleon and its different modes of excitation, the baryon resonances. Initially, most of the information on these excitations came primarily from partial wave analysis of data from πN scattering. Recently, these data have been supplemented by a large amount of information from pion electro- and photoproduction experiments. Yet, in spite of extensive studies spanning decades, many of the baryon resonances are still not well established and their parameters (i.e., mass, width, and couplings to various decay modes) are poorly known. Much of this is due to the complexity of the nucleon resonance spectrum, with many broad, overlapping resonances. Available experimental data consist mainly of differential cross sections and very little data for polarization observables. The cross section data alone are not sufficient for a deconvolution of a complex baryon resonance spectrum. One can hardly expect significant progress without extensive information about polarization observables.

We propose to measure with CLAS and the photon tagger in Hall B of Jefferson Lab the observables Σ, T, P, E, F, G, and H in η-photoproduction with a polarized photon beam and polarized frozen spin target for photon energies 0.75 – 2.0 GeV. We will pay a special attention to the range of W 1.5 – 1.8 GeV where there are eight known resonances. We will use finer binning in this range. We will use 25 MeV wide bins in photon energy for energies below 1.4 GeV and 50 MeV wide bins above 1.4 GeV. We will use 10 angular bins within $\cos\theta_{\mathrm{c.m.}}$ range from -0.9 to 0.9. Expected statistical accuracy for all observables is 0.05 – 0.1. This experiment will contribute over 300 data points for each of the seven polarization observables, or over 2000 data points total. Note that the world database currently has a total of 225 data points with polarization.

These measurements will provide an extensive data set with good statistical accuracy and well understood systematic uncertainties. This data will provide stringent tests of models of the nucleon, and provide a definitive data set for nucleon resonance spectrum analyses. The proposed experimental program is a natural continuation of research started in the initial η photoproduction experiment, E91-008. *Together with experiments E02-112, E03-105 and E04-102, we will mount a package of experiments that will provide essential data of unprecedented quality and kinematical coverage suitable for coupled-channels analysis, one of the milestones in hadronic physics.*

Contents

1 Motivation

Among the most exciting and challenging topics in subnuclear physics today is the study of the structure of the nucleon and its different modes of excitation, the baryon resonances. Initially, most of the information on these excitations came primarily from partial wave analysis of data from πN scattering. Recently, these data have been supplemented by a large amount of information from pion electro- and photoproduction experiments. Yet, in spite of extensive studies spanning decades, many of the baryon resonances are still not well established and their parameters (i.e., mass, width, and couplings to various decay modes) are poorly known. Much of this is due to the complexity of the nucleon resonance spectrum, with many broad, overlapping resonances coupling to the πN channel.

The importance of this topic is also illustrated by the fact that the U.S. Department of Energy lists as one of the top 10 milestones in hadronic physics *"To complete the combined analysis of available data on single π, η, and K photo-production of resonances and incorporate the analysis of two-pion final states into the coupled-channel analysis of resonances."* For this milestone to be reached requires that polarization observables for these reactions be measured. Jefferson Lab has played a leading role in determining the properties of these reactions, and can continue this leadership role by facilitating measurements of the polarization observables. Theorists are already developing the necessary tools to perform such an analysis.

While traditional theoretical approaches have highlighted a semi-empirical approach to understanding the process as proceeding through a multitude of s-channel resonances, t-channel processes, and non-resonant background (as discussed in, for example, Ref. [1]), more recently attention has turned to approaches based on the underlying constituent quarks. An extensive review of the quark models of baryon masses and decays can be found in Ref. [2]. While these quark approaches are more fundamental and hold great promise, all of them predict many more resonances than have been observed, leading to the so-called "missing resonance" problem.

Additional progress in pinning down the details of the nucleon resonance spectrum can be made by looking at reaction channels and observables which select particular resonances from the spectrum. In this regard, photoproduction of η-mesons provides a valuable "isospin filter" for the baryon resonance spectrum. Because of the quantum numbers of the η-meson, this process directly couples to isospin $I = \frac{1}{2}$ resonances only. This has led to significant activity in recent years on electro- and photoproduction of these mesons.

While these experiments have established that the $S_{11}(1535)$ resonance dominates the reaction near threshold, there are nonetheless many questions concerning its properties, such as why the $S_{11}(1535)$ couples so strongly to ηN channel while higher mass resonances couple so weakly. Furthermore, as more data on η production have become available, comparisons with properties determined from pion production results have revealed apparent discrepancies. Two such examples involve the helicity amplitudes for this resonance, which had been thought to be well established from the existing pion photoproduction data. As pointed out in the recent edition of the Review of Particle Physics[3], fits to η photoproduction data have given $N\gamma$ amplitudes for $S_{11}(1535)$ that are substantially larger than those extracted from fits to π-production data. More recent analyses [4, 5] have considered the sensitivity of this reaction to contributions from the $D_{13}(1520)$. The ratio of $D_{13}(1520) \rightarrow N\gamma$ amplitudes $A_{3/2}/A_{1/2}$ was found to be $-2.5 \pm 0.5 \pm 0.4$ in [4] and -2.1 ± 0.2 in [5]. Results inferred from π photoproduction are about a factor of three larger in magnitude [6]. The η photoproduction result is particularly surprising, as the $D_{13}(1520)$ has a very clean resonance signature in π photoproduction. Recent analysis of π and η electroproduction data from CLAS finds no discrepancy at Q^2=0.4 and 0.65 GeV/c^2 [7]. Thus, despite the dominance of the $S_{11}(1535)$ resonance near threshold, its relatively large cross section and the growing database from η electro-

Table 1. The status of the N and Δ resonances. Only those with an overall status of $***$ or $****$ are included in the main Baryon Summary Table.

Particle	$L_{2I\cdot 2J}$	Overall status	Status as seen in —						
			$N\pi$	$N\eta$	ΛK	ΣK	$\Delta\pi$	$N\rho$	$N\gamma$
$N(939)$	P_{11}	****							
$N(1440)$	P_{11}	****	****	*			***	*	***
$N(1520)$	D_{13}	****	****	*			****	****	****
$N(1535)$	S_{11}	****	****	****			*	**	***
$N(1650)$	S_{11}	****	****	*	***	**	***	**	***
$N(1675)$	D_{15}	****	****	*	*		****	*	****
$N(1680)$	F_{15}	****	****				****	****	****
$N(1700)$	D_{13}	***	***	*	**	*	**	*	**
$N(1710)$	P_{11}	***	***	**	**	*	**	*	***
$N(1720)$	P_{13}	****	****	*	**	*	*	**	**
$N(1900)$	P_{13}	**	**					*	
$N(1990)$	F_{17}	**	**	*	*	*			*
$N(2000)$	F_{15}	**	**	*	*	*	*	**	
$N(2080)$	D_{13}	**	**	*	*				*
$N(2090)$	S_{11}	*	*						
$N(2100)$	P_{11}	*	*	*					
$N(2190)$	G_{17}	****	****	*	*	*		*	*
$N(2200)$	D_{15}	**	**	*	*				
$N(2220)$	H_{19}	****	****	*					
$N(2250)$	G_{19}	****	****	*					
$N(2600)$	$I_{1\,11}$	***	***						
$N(2700)$	$K_{1\,13}$	**	**						
$\Delta(1232)$	P_{33}	****	****	F				****	
$\Delta(1600)$	P_{33}	***	***	o		***	*	**	
$\Delta(1620)$	S_{31}	****	****	r		****	****	***	
$\Delta(1700)$	D_{33}	****	****	b	*	***	**	***	
$\Delta(1750)$	P_{31}	*	*	i					
$\Delta(1900)$	S_{31}	**	**	d	*	*	**	*	
$\Delta(1905)$	F_{35}	****	****	d	*	**	**	***	
$\Delta(1910)$	P_{31}	****	****	e	*	*	*	*	
$\Delta(1920)$	P_{33}	***	***	n	*	**		*	
$\Delta(1930)$	D_{35}	***	***		*			**	
$\Delta(1940)$	D_{33}	*	*	F					
$\Delta(1950)$	F_{37}	****	****	o	*	****	*	****	
$\Delta(2000)$	F_{35}	**		r			**		
$\Delta(2150)$	S_{31}	*	*	b					
$\Delta(2200)$	G_{37}	*	*	i					
$\Delta(2300)$	H_{39}	**	**	d					
$\Delta(2350)$	D_{35}	*	*	d					
$\Delta(2390)$	F_{37}	*	*	e					
$\Delta(2400)$	G_{39}	**	**	n					
$\Delta(2420)$	$H_{3\,11}$	****	****					*	
$\Delta(2750)$	$I_{3\,13}$	**	**						
$\Delta(2950)$	$K_{3\,15}$	**	**						

and photoproduction experiments, our understanding of this resonance remains ambiguous, even though it is assigned a "4 star" status by the Particle Data Group.

Our knowledge of the coupling of the higher mass N^* resonances to the ηN channel is even more limited. Table 1, taken from the Particle Data Group Review of Particle Physics, illustrates very well the current status of our knowledge of the N^* resonances: Only *two* of the 22 suggested N^* resonances have more than one "star" for the ηN channel, whereas 14 of those 22 resonances are known in the πN with *three or four* stars.

One of the obstacles in determining the couplings of the baryon resonances to $N\eta$ is that the coupling is generally very small. As a result, differential cross section data, though helpful, still provide a very limited exploitation of this "isospin filter" tool. Despite these small couplings, however, these resonances should reveal themselves more clearly through the interference with dominant amplitudes. These interference terms can be isolated via polarization observables. The formalism and terminology for the various polarization observables of interest in η photoproduction

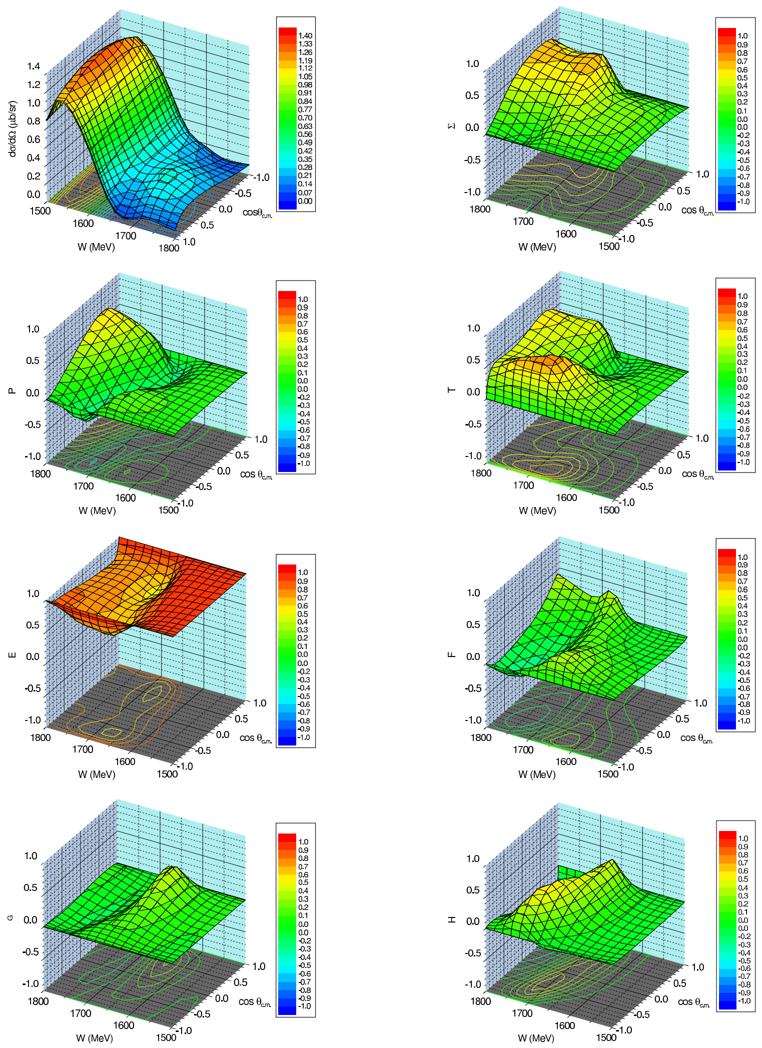

Figure 1: Predictions of ETA-MAID[1] for all polarization observables from the polarized photon beam/polarized target group of experiments.

are described in the Appendix.

Figure 1 shows predictions of ETA-MAID [1] for all observables from the polarized beam/polarized target (denoted BT in the Appendix) group. The calculations shown include the $S_{11}(1535)$, $S_{11}(1650)$, $P_{11}(1710)$, $P_{13}(1720)$, $D_{13}(1520)$, $D_{13}(1700)$, $D_{15}(1675)$, and $F_{15}(1680)$ resonances. The predictions display that, under the assumed resonances, couplings, and relative phases, there is much variation in magnitude for each of the observables over the measurable region. These variations should be readily measurable with the equipment we discuss below, and thus providing a powerful tool for deconvolution of the resonance spectrum.

Figure 2 and Table 2 show the coverage in photon energy E_γ and scattering angle $\theta_{\mathrm{c.m.}}$ of the available experimental data on η photoproduction, and also the total number of data points for various observables. The left-hand panel contains points indicating where differential and total cross sections exist. The database is dominated by four experiments: data from TAPS [8] near threshold (green triangles, 100 data points), data from GRAAL [9] (blue squares, 244 data points)

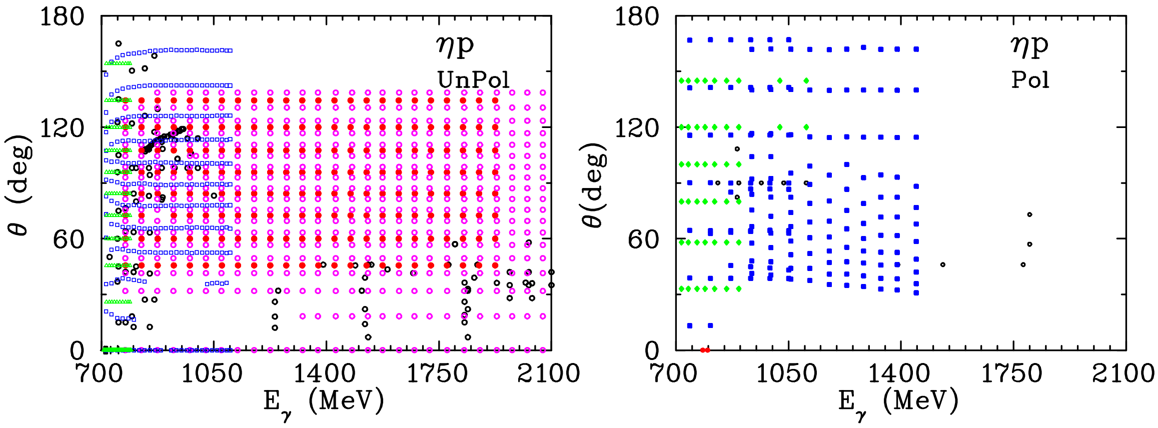

Figure 2: World database for η photoproduction. Symbols are explained in text.

and data from CLAS [10] (red circles, 182 data points). In addition to the points just described, the figure includes data from CB-ELSA that is still in preprint form [11] (magenta circles, 383 data points). The total number of unpolarized data points is 1086. The right-hand panel similarly shows available polarization data, dominated by two data sets: beam asymmetry Σ measurements from GRAAL [12] (blue squares, 166 data points) and target asymmetry T measurements from ELSA [13] (green diamonds, 50 data points). Besides these six experiments that contribute the majority of the data, there are an additional smaller number of points from from several other experiments.

Table 2: Number of data points for different observables.

Observable	Number of points
σ_{tot}	66
$d\sigma/d\Omega$	1020
P	7
Σ	166
T	50
Helicity asymmetry	2
Total	1311

It is important to note that, of all these polarization observables (225 points), none are of the double polarization type. One can see that the coverage for cross sections as a function of photon energy and scattering angle is now rather good from threshold up to 2 GeV, with the exception of the most forward and most backward angles. On the other hand, polarization observables have been mainly measured in the region of $S_{11}(1535)$ resonance. Above that resonance exists a "desert" where models have considerable ambiguity, since many combinations of resonances can account for the available cross section data. Consequently, it is not surprising that we know little about the coupling of resonances above $W = 1.6$ GeV to $N\eta$. Also worth noting is that all available models have trouble describing the target asymmetry T data at low energy. *With cross section data alone, there simply is insufficient information to extract resonance parameters.*

Using CLAS and the photon tagger, we provided new data on the differential cross sections for the reaction $\gamma p \to \eta p$ [10]. These new data illustrate the limitations of cross sections alone. The measured differential cross sections are presented in Fig. 3. In general, agreement between the new

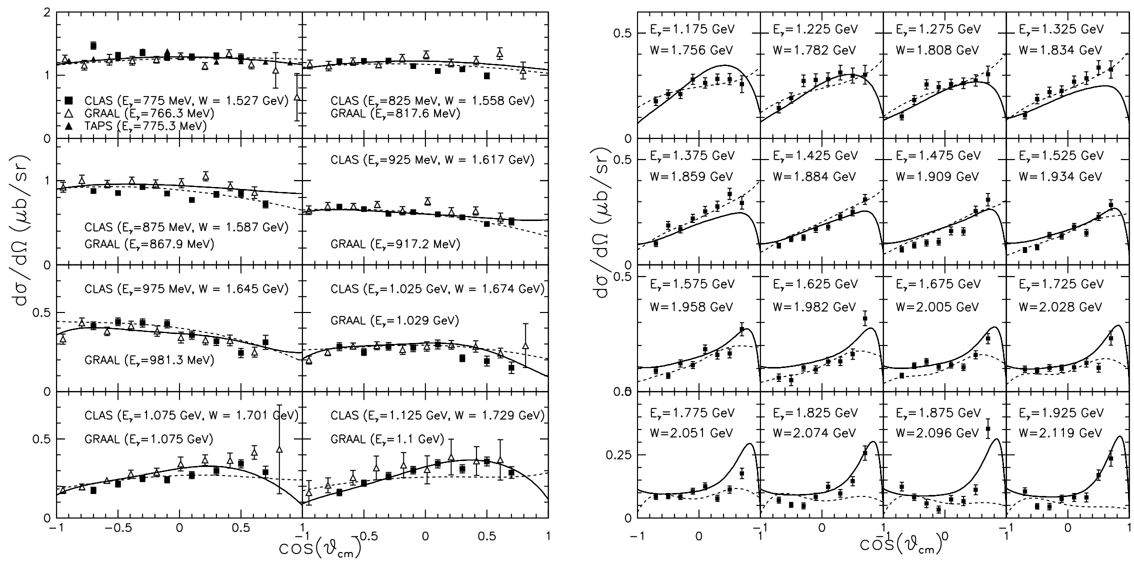

Figure 3: Differential cross section for $\gamma p \to p\eta$ measured with CLAS. Other results from TAPS[8] and GRAAL[9] are shown for comparison. Also shown are prediction from Refs. [1] (solid line) and [14] (dashed line).

CLAS data and previous experiments is very good. This new data set extends to the previously unmeasured range of W from 1.7 to 2.1 GeV.

Figure 4 shows a comparison of the estimated total cross section with new predictions from both ETA-MAID[1] (REM) and from the chiral quark model of Saghai and Li[14] (χQM). The preliminary results of this new ETA-MAID fit generally reproduce the shapes of the observed cross sections quite well, including the forward peak seen at the highest energies, usually interpreted as being due to t-channel processes. However, while the REM shapes mimic what we observed, those calculations fall below our differential cross sections around W=1.85 GeV, and are noticeably above our data at $W \geq$1.9 GeV. With respect to the new χQM predictions, those calculations are generally in very good agreement with our data for $W \leq 1.9$ GeV. The inclusion of a third S_{11} resonance not predicted by the $SU(6)\otimes O(3)$ quark model in these preliminary calculations, with a mass 1.79 GeV and width of 250-350 MeV, markedly improved the fit to our data[14]. The agreement between our data and the χQM around W=1.85 GeV is considerably better than with the REM results. However, above W=1.9 GeV, the χQM approach begins to fall below our data, and the predicted shapes are inconsistent with the peak at forward angles in the differential cross section as the energy increases. This disagreement suggests additional resonances beyond those included in the χQM approach may be needed, and t-channel contributions not incorporated directly in that model may also be important.

These new cross sections certainly have provided some insight and direction for these two theoretical approaches. Both approaches show regions of greater and lesser success, and the choice of which resonances are included in the ETA-MAID approach is particularly poorly constrained. It is worth reiterating that, as seen above, the models are having different degree of success in reproducing the measured differential cross sections in different kinematical regions and do not always agree with each other and the data. They certainly will be tested much more stringently with various asymmetries. *Polarization observables are essential for making more progress in extracting of coupling parameters for various resonances.*

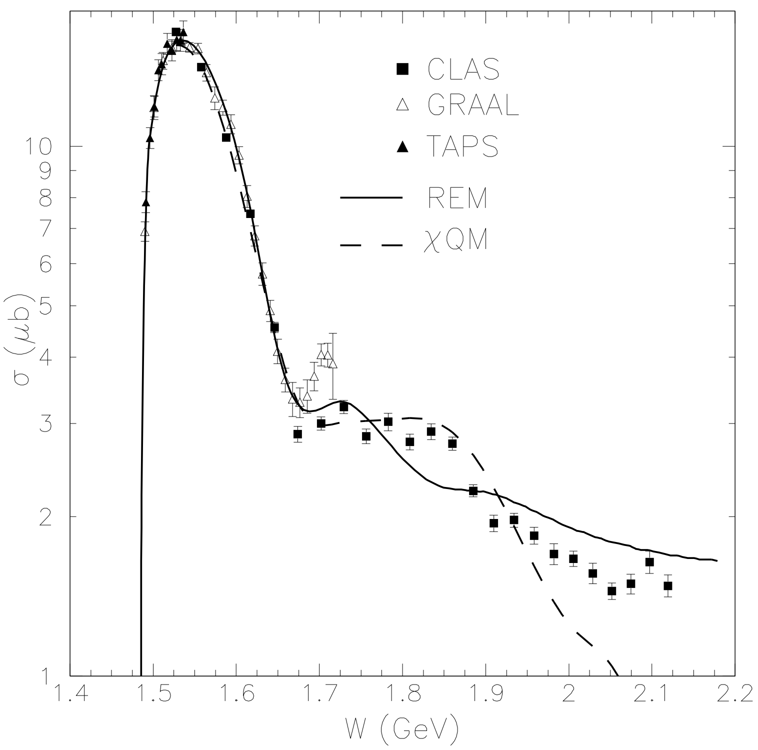

Figure 4: Total cross section estimates. Results from TAPS[8] and GRAAL[9] are shown for comparison. Curves are as in Fig. 3.

Overall, there are 16 different polarization observables for real photon experiments, and there are four independent helicity amplitudes. While several papers have been devoted to discussing a so-called "complete experiment" [15, 16, 17], there is no simple universal recipe for which observables and how accurately need to be measured for an unambiguous amplitude reconstruction. In general, if the unpolarized cross section and single spin observables Σ, P and T are measured, one can reconstruct moduli of all four complex helicity amplitudes. However, their relative phases could not be unambiguously reconstructed. While single polarization observables are sensitive to the moduli of amplitudes, double polarization observables reflect their interference and thus could be used as a tool to measure their relative phases. As was shown in Ref. [16], in addition to unpolarized cross sections and single spin polarizations Σ, P and T, one needs *at least* four double spin observables. It was also shown that if all four are from the same group (either BT, BR or TR, as defined in the Appendix), ambiguities cannot be resolved. While the idea of a "complete experiment" and direct amplitude reconstruction sounds very attractive, accomplishing this goal is quite difficult: one needs to measure at least eight observables at each energy.

One method of extracting information from such data in a less model-dependent way than, say, the ETA-MAID or χQM approaches, is the partial wave analysis epitomized by the SAID technique [6, 18]. Originally these analyses were developed for NN and πN processes, but they have now been extended to meson (π, η, K) electro- and photoproduction data. In this approach, each of the helicity amplitudes is expressed in terms of multipoles. Multipoles, in turn, are functions of photon energy with a few adjustable parameters. These parameters are determined from the best fit to all available experimental data with some additional theoretical constraints. This approach allows the incorporation all available observables from different experiments at different energies and angles into one data set and to account for their systematic uncertainties by means of adjustable normalization factor specific for each experiment. Which multipoles must be included is not known a priori. It depends on the experimental data. *Polarization data are crucial for this procedure, since without them, the solution is poorly constrained.*

2 Proposed experimental setup

Hall B provides a unique set of instruments for these experiments. One instrument is the CLAS [19], a large acceptance spectrometer which allows detection of particles in a wide range of θ and ϕ. The other instrument is a broad-range photon tagging facility [20] with the recent addition of the ability to produce linearly-polarized photon beams through coherent bremsstrahlung. The remaining component essential for the proposed experiment is a frozen-spin polarized target, which is now under construction.

2.1 Tagged photon beam

The Hall B photon tagger [20] covers a range in photon energies from 20 to 95% of the incident electron beam energy. Unpolarized, circularly-polarized and linearly-polarized tagged photon beams are presently available.

2.1.1 Circularly-polarized photon beam

With a polarized electron beam incident on the bremsstrahlung radiator, a circularly-polarized photon beam can be produced. The degree of circular polarization of the photon beam depends on the ratio $k = E_\gamma/E_e$, and is given by [21]

$$P_\odot = P_e \cdot \frac{4k - k^2}{4 - 4k + 3k^2}. \tag{1}$$

The quantity $P_\odot$ ranges from 60% to 99% of the incident electron beam polarization P_e for photon energies E_γ between 50% and 95% of the incident electron energy.

2.1.2 Linearly-polarized photon beam

A linearly-polarized photon beam is produced by the coherent bremsstrahlung technique, using an oriented diamond crystal as a radiator. This technique was used successfully during the CLAS-g8a running period. Figure 5 shows an example of an uncollimated, linearly polarized tagged photon spectrum obtained in Hall B.

The degree of polarization is a function of the fractional photon beam energy and collimation and can reach 80% to 90%. With linearly polarized photons, over 80% of the photon flux is confined to a 200-MeV wide energy interval.

2.2 Frozen spin target

An essential piece of the hardware for this experiment, together with other approved experiments E02-112 [22], E03-105 [23] and E04-102 [24], is a polarized target capable of being polarized transversely and longitudinally with a minimal amount of material in the path of outgoing charged

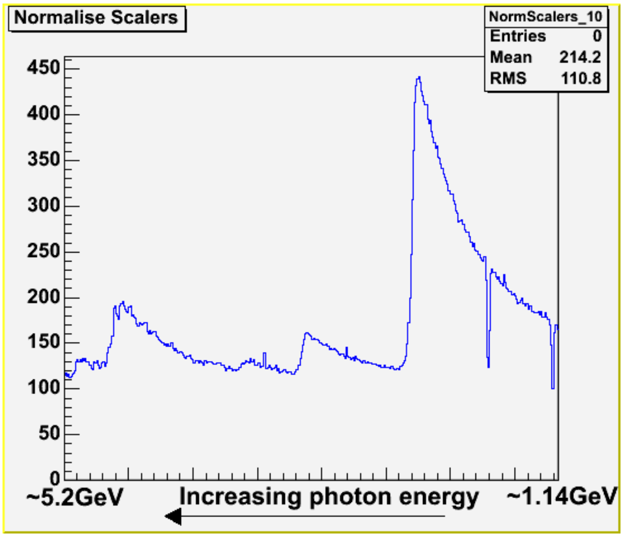

Figure 5: Coherent bremsstrahlung spectrum.

Table 3: Target properties.

Chemical formula	C_4H_9OH
Dilution factor	10/74
Length	50 mm
Diameter	15 mm
Density	0.985 g/cm^3
Packing factor	0.62

particles. The existing Hall B polarized target [25] used in electron beam experiments is a dynamically polarized target. The target is longitudinally polarized with a pair of 5 Tesla Helmholtz coils. These massive coils limit available aperture to 55 degrees in forward direction. For photon beam experiments, a frozen-spin target is a much more attractive choice.

In frozen-spin mode, the target material is dynamically polarized in a strong magnetic field of 5 Tesla at the temperature of 1K outside of CLAS. After maximal polarization is reached the cryostat is turned to the "holding" mode with much lower magnetic field of 0.5 Tesla at a temperature of 50 mK, and then moved in CLAS. A photon beam does not induce noticeable radiation damage and does not produce significant heat load on the target material. Under these conditions the target can hold its polarization with a relaxation time on the order of several days before re-polarization is required. Since the holding field is relatively low, it is possible to design a "transparent" holding magnet with a minimal amount of material for the charged particles to traverse on their way into CLAS. The target system will use an external polarizing magnet located outside of CLAS, and an internal holding magnet inside the cryostat.

The target cell will be 50 mm long and 15 mm in diameter. Presently we are planning to use butanol as the target material. The planned target material properties are summarized in Table 3.

The design and construction work for the Hall B frozen-spin target is being done by the JLab target group with the help of users, and is well underway. The current plan is to have the target operational and ready for experiments by the end of 2005.

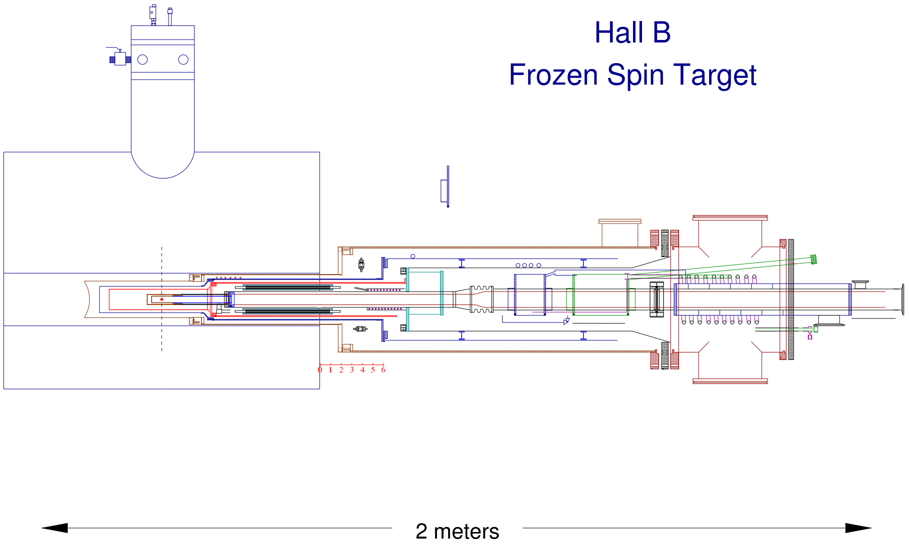

Figure 6: Schematics of the Hall B frozen spin target.

2.2.1 Polarizing magnet

A horizontal 5.0 Tesla superconducting polarizing magnet with a 130 mm warm bore has been purchased from Cryomagnetics, Inc. The magnet operates very reliably. A precise NMR measurement of its field map was performed when the magnet arrived at JLab. The details of these measurements are described in Ref. [26]. This measurement confirmed that the homogeneity of the magnetic field within the target volume (20 mm in diameter and 50 mm long) is better than 40 ppm. This degree of homogeneity allows the use of a broad variety of target materials, including some with very narrow EPR lines.

2.2.2 Dilution refrigerator

For a cylindrical target volume with a 15 mm diameter and a 50 mm length, approximately 20 mW of microwave power will be necessary for the polarization process at 0.5 K, with a polarization build-up time of about 30 minutes. Under experimental run conditions the heat load from the photon beam is about 1 μW. This implies that, in frozen spin mode at 0.5 Tesla at 50 mK, the refrigerator should provide a cooling power of a few μW. The only technique that satisfies these conditions is a ^{3}He/^{4}He dilution refrigerator. The refrigerator is currently under design and construction by the JLab Polarized Targets Group. Figure 6 shows the target cryostat inserted in the polarizing magnet. Figure 7 is an expanded view of the target cell region. The cell is inside the mixing chamber, which in turn is inside the holding solenoid.

2.2.3 Holding magnets

The internal holding system should be as "transparent" to outgoing particles as possible. This demands limiting the amount of conductor, which results in a lower intensity holding field. By contrast, the relaxation time of polarization is a strong function of the magnetic field intensity; a

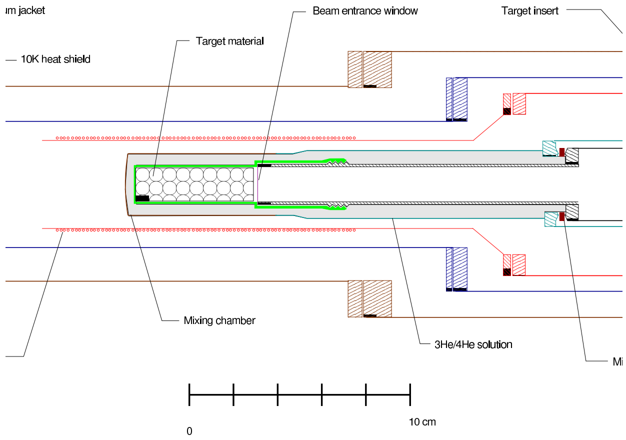

Figure 7: Expanded view of the central region of the Hall B frozen spin target.

higher field maintains the polarization longer. We considered a holding field of about 0.5 Tesla. In order to be able to monitor the degree of polarization during experimental running, the homogeneity of the holding field within the target cell volume must be better than 1%.

This experiment demands both longitudinal and transverse target polarizations. Therefore, we need two different holding magnets. We performed an extensive simulation to find the optimal design for a holding magnet system using the Poisson/Superfish 2D package [27] and the Opera-3D package [28]. Details of this study can be found in Ref. [29].

For the longitudinal holding field, we considered a solenoid. The simulation shows that a design with three layers of 0.112 mm diameter NbTi superconducting wire can provide a central field intensity of up to 0.5 Tesla, with the homogeneity over the entire target cell volume better than 0.5%. This homogeniety will allow us to monitor the target polarization via NMR while in the frozen spin mode. Tests of a prototype coil yielded results that confirm the simulation.

For the transverse holding magnet we considered a dipole magnet with race-track shaped coils wrapped around the cylinder. The simulation shows that with three or four layers of superconducting wire, we can expect field homogeneity better than 0.8%. Prototyping of this design is underway.

2.3 CLAS configuration

We will use the CLAS detector in its standard configuration for the photon beam running. The frozen spin target will be placed in the center of CLAS, and surrounded with the new start counter. We will run with the torus magnetic field set to one-half of the maximum field, outbending positive particles. The trigger for this experiment requires the detection of at least one charged particle in CLAS. This configuration is compatible with all other proposed experiments using the frozen spin target.

3 Run conditions and analysis technique

The formalism for the various cross sections measured is presented in the Appendix. (All the equations for the cross section presented in the Appendix are in the reaction frame.) Figure 8 shows the relative orientation of the reaction frame, laboratory frame, beam, and target polarization. We use the following notation:

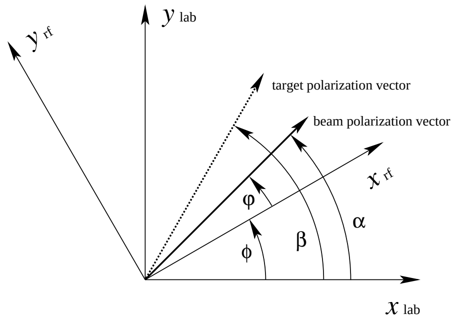

Figure 8: Coordinate frames for polarization vectors in η photoproduction in the laboratory system.

φ - angle between reaction plane and beam polarization plane;

ϕ - angle of the reaction plane in the lab frame;

α - angle of beam polarization plane in the lab frame;

β - angle of the transverse target polarization in the lab frame.

The direction of the Z-axis is the same in all coordinate frames and is defined by incident photon momentum. Then, the target polarization in the reaction frame will be:

$$\begin{aligned} P_x &= P_t^{\text{lab}} \cdot \cos(\beta - \phi) \\ P_y &= P_t^{\text{lab}} \cdot \sin(\beta - \phi) \\ P_z &= P_z^{\text{lab}}, \end{aligned}$$

where P_t^{lab} is the degree of transverse target polarization and P_z^{lab} is the degree of longitudinal target polarization. We can write Eq. 9 of the Appendix for different beam/target combinations in the laboratory frame in the following ways (all symbols are defined in the Appendix):

Linearly polarized beam, transverse target:

$$\begin{aligned} \frac{1}{\sigma_0}\frac{d\sigma}{d\Omega} &= 1 - P_T\Sigma\cos 2(\alpha - \phi) \\ &\quad - P_t^{\text{lab}}\cos(\beta - \phi)P_T H \sin 2(\alpha - \phi) \\ &\quad - P_t^{\text{lab}}\sin(\beta - \phi)(-T + P_T P \cos 2(\alpha - \phi)). \end{aligned} \tag{2}$$

Linearly polarized beam, longitudinal target:

$$\begin{aligned} \frac{1}{\sigma_0}\frac{d\sigma}{d\Omega} &= 1 - P_T\Sigma\cos 2(\alpha - \phi) \\ &\quad + P_T P_z^{\text{lab}} G \sin 2(\alpha - \phi). \end{aligned} \tag{3}$$

Circularly polarized beam, transverse target:

$$\begin{aligned} \frac{1}{\sigma_0}\frac{d\sigma}{d\Omega} &= 1 + P_t^{\text{lab}}\cos(\beta - \phi)P_\odot F \\ &\quad + P_t^{\text{lab}}\sin(\beta - \phi)T. \end{aligned} \tag{4}$$

Circularly polarized beam, longitudinal target:

$$\frac{1}{\sigma_0}\frac{d\sigma}{d\Omega} = 1 - P_z^{\text{lab}} P_\odot E. \tag{5}$$

Thus, the proposed experimental program will consist of four experiments with different combinations of beam and target polarizations:

(A) Linearly-polarized beam – transversely-polarized target:
Measurements of Σ,H, P, T (see Eq. (2));

(B) Linearly-polarized beam – longitudinally-polarized target:
Measurements of Σ,G (see Eq. (3));

(C) Circularly-polarized beam – transversely-polarized target:
Measurements of F, T (see Eq. (4));

(D) Circularly-polarized beam – longitudinally-polarized target:
Measurements of E (see Eq. (5)).

Setting (A) with linearly polarized beam and transversely polarized target is the most interesting. I gives an access to four different observables in one measurement.

In order to achieve maximum acceptance and efficiency for the reaction $\gamma + p \to \eta + p$ we will detect the recoil proton in CLAS and use the missing mass technique to identify η-photoproduction events, the same method as we used to obtain the data shown in Figs. 3 and 4 [10]. With this approach an angular coverage depends on the recoil proton momentum determination and is limited to $\cos\theta_{\rm c.m.}$ range from -0.9 to 0.9, by the effects of energy losses in the target and detector material, multiple Coulomb scattering in detector elements, and geometry of the CLAS detector. However, this angular range is more than sufficient to provide very stringent tests on any currently existing model or approach. Within this range the efficiency of the CLAS to the η-photoproduction events is about 0.6 and is flat and is almost independent on the incident photon energy.

To extract polarization observables we are going to use the same procedure as described in the approved pion photoproduction experiment E03-105 [23]. Here is an outline of the procedure.

The experimentally observed angular distribution, $A_{\rm exp}(\phi)$, is the weighted sum of the distributions coming from polarized protons and other (unpolarized) target materials:

$$A_{\rm exp} = \frac{A_{\rm pol}N_{\rm pol} + A_{\rm unpol}N_{\rm unpol}}{N_{\rm pol} + N_{\rm unpol}} \tag{6}$$

The target nuclei ^{12}C and ^{16}O have spin 0, and are unpolarized; thus, for all target and beam/target polarization observables, the asymmetry $A_{\rm unpol}$ vanishes. Knowing the dilution factor $f_{\rm eff} = N_{\rm pol}/(N_{\rm pol} + N_{\rm unpol})$, the asymmetry of interest can be extracted as

$$A_{\rm pol} = \frac{1}{f_{\rm eff}} A_{\rm exp} \ . \tag{7}$$

The polarization observables of interest can be extracted by means of a Fourier analysis of the experimental azimuthal angular distribution. The estimator and the standard uncertainty is given by

$$O = \frac{1}{f} \cdot \frac{\sum w_i}{\sum w_i^2} \quad \text{and} \quad u(O) = \frac{1}{f}\sqrt{\frac{\kappa}{N}} \ , \tag{8}$$

where the sums are running over all events in the considered kinematical bin and O stands for the observable (E, T, Σ, G, F, H, or P). The standard uncertainty depends on the total number of events in that bin, $N = N_{\rm pol}/f$, and a scale factor κ. The factor κ accounts for differences in the way observables enter the cross section Eqs. (2) – (5); for no angular dependence ($\kappa = 1$), as a

Table 4: Extraction of target and beam/target polarization observables from azimuthal angular distributions.

Observable	Weight w_i	f	κ
E	$-h_i$	$P_\odot P_z^{\rm lab} f_{\rm eff}$	1
T	$\sin(\beta_i - \phi_i)$	$P_t^{\rm lab} f_{\rm eff}$	2
Σ	$-\cos 2(\alpha_i - \phi_i)$	$P_T P_{XY}^{\rm lab} f_{\rm eff}$	2
G	$\sin 2(\alpha_i - \phi_i)$	$P_T P_t^{\rm lab} f_{\rm eff}$	2
F	$h_i \cos(\beta_i - \phi_i)$	$P_\odot P_t^{\rm lab} f_{\rm eff}$	2
H	$-\cos(\beta_i - \phi_i)\sin 2(\alpha_i - \phi_i)$	$P_T P_t^{\rm lab} f_{\rm eff}$	4
P	$-\sin(\beta_i - \phi_i)\cos 2(\alpha_i - \phi_i)$	$P_T P_t^{\rm lab} f_{\rm eff}$	4

single Fourier coefficient ($\kappa = 2$), or as a linear combination of two Fourier coefficients ($\kappa = 4$). The weights w_i, dilution factors f, and scale factors are different for each observable, and given in Table 4.

Since all three polarization observables T, H, and P have Fourier components in the first order of $\sin\phi$ or $\cos\phi$, it is mandatory to take data with beam and/or target polarizations flipped to disentangle these observables.

3.1 Background

There are two main sources of background (and hence systematic uncertainties) associated with this technique.

- Multipion production
- Reactions on bound nucleons of the target material

We performed a Monte Carlo simulation for both sources of the background. We used the **genbos** event generator to produce events for all considered reactions. This generator is an adaptation for CLAS of the code described in Ref. [32]. For the reactions where angular distribution is known it generates events according to this distribution. If an angular distribution is not known it generates events according to the phase space.

In addition we developed event generator to simulate η photoproduction on a free nucleon. It uses the SAID partial wave analysis predictions for all observables to generate angular distributions, both in θ and ϕ.

All generated reaction channels were processed through GSIM (full GEANT simulation of CLAS detector). We present here the results for incident photon energy $E_\gamma = 1.1$ GeV, which corresponds to a W of about 1.72 GeV. We generated 100K events for each reaction channel considered.

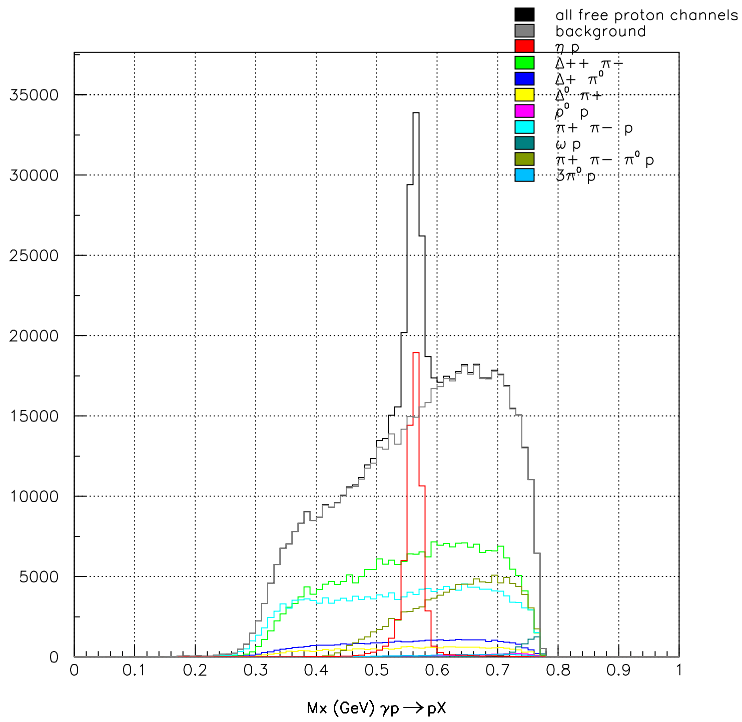

Figure 9: Missing mass spectra from the reactions on a free nucleon.

To estimate the background from reactions on free protons, we included the following reactions:

$$
\begin{aligned}
\gamma + p &\rightarrow \Delta^{++} + \pi^- \\
\gamma + p &\rightarrow \Delta^{+} + \pi^0 \\
\gamma + p &\rightarrow \Delta^{0} + \pi^+ \\
\gamma + p &\rightarrow p + \pi^+ + \pi^- \\
\gamma + p &\rightarrow p + \rho^0 \\
\gamma + p &\rightarrow p + \pi^+ + \pi^- + \pi^0 \\
\gamma + p &\rightarrow p + 3\pi^0 \\
\gamma + p &\rightarrow p + \omega
\end{aligned}
$$

Missing mass spectra for the reaction $\gamma + p \rightarrow p + X$ are presented in Fig. 9. It shows contributions to the total yield from various reaction channels. The contributions from different channels are weighted by their cross sections.

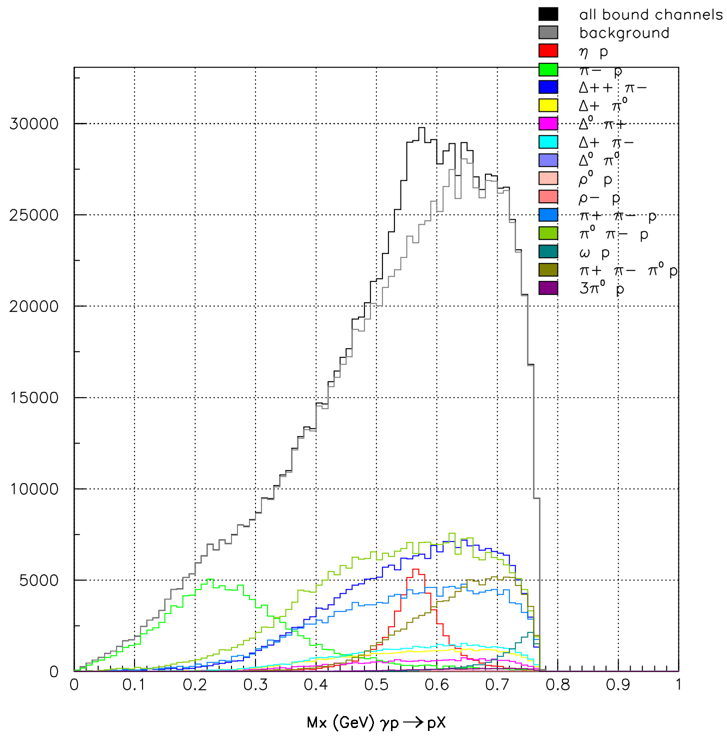

Figure 10: Missing mass spectra from the reactions on a bound nucleon.

For the reactions on bound nucleons, in addition to these channels we added reactions on the neutron which have a proton in the final state:

$$
\begin{aligned}
\gamma + n &\rightarrow p + \pi^- \\
\gamma + n &\rightarrow \Delta^+ + \pi^- \\
\gamma + n &\rightarrow \Delta^0 + \pi^0 \\
\gamma + n &\rightarrow p + \pi^0 + \pi^- \\
\gamma + n &\rightarrow p + \rho^-
\end{aligned}
$$

In this case, the momentum of the target nucleon was generated according to the Fermi momentum distribution. Figure 10 shows the missing mass distribution, assuming the reaction $\gamma + p \rightarrow p + X$ on the bound nucleons. As in the case of a free nucleon, we sum these with weights proportional to the cross section on a free nucleon. Then we sum over all backgrounds on free and bound nucleons. The background from bound nucleons was scaled by the ratio of bound/free nucleon number in the target material. This is a somewhat conservative estimate. Usually a cross section on nuclei scales as $A^{2/3}$ compared to free nucleons.

The final sum of all simulated backgrounds together with η production on a free proton is shown in Fig. 11. One can see that the reaction of interest is clearly identifiable. If we apply a kinematical cut on the missing mass around η as shown in Fig. 12, we get a signal to background ratio of about 0.17 within this range. This ratio represents an estimate of an effective dilution factor f in table 4 which will be used in the analysis. In the real experiment we will determine this factor from the data in each kinematical bin. Our simple model for nuclear background does not include final

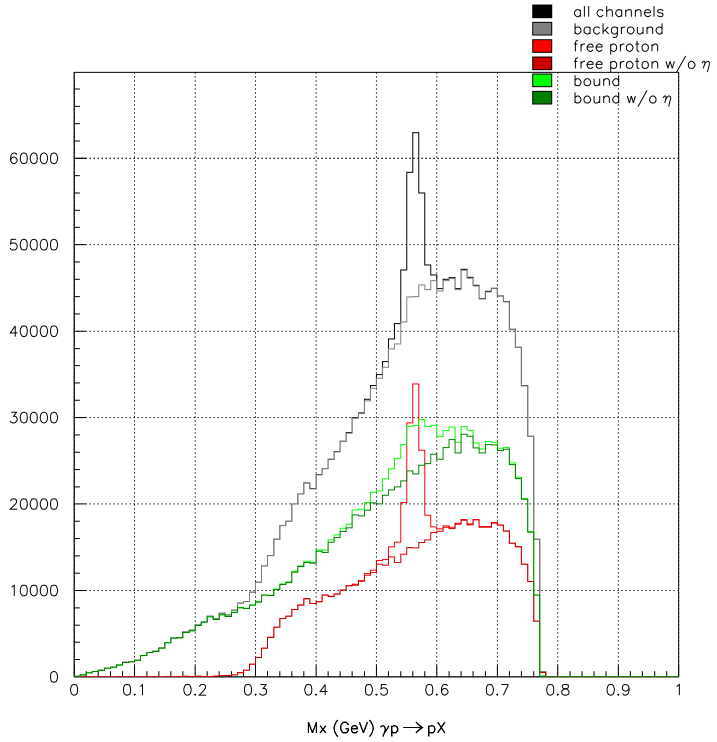

Figure 11: All reactions on free and bound nucleons.

state interaction and rescattering. There is a chance that we can reduce nuclear background in the analysis of real experimental data by applying additional event selection criteria and kinematical cuts, for instance rejection of events where more than one proton detected in CLAS.

The background reactions on a free proton can have their own asymmetry. Since we have no knowledge of what that asymmetry might be, we assumed no asymmetry in this simulation. In the analysis of the real experimental data we will evaluate and subtract background in each kinematical bin. In order to get a better handle on the background from bound nucleons, we are planning to install an additional carbon target with a thickness of about 10-20% of the main target, located a few centimeters downstream of the polarized target. With this configuration, we will measure simultaneously events from both targets. In the analysis, we can clearly separate events coming from both targets using vertex information.

3.2 Rates and uncertainties estimate

There are several factors which put a limit on the maximum luminosity that can be used in the experiment. The most important of them are maximum CLAS DAQ rate, maximum rate per tagger T-counter and rate of accidental coincidence in the tagger. We are planning to run with the collimated photon beam. For circularly polarized beam the diameter of the collimator will be 2.6 mm. The tagging ratio with this collimation will be about 0.2 and 0.4 at electron beam energy of 1.6 and 2.2 GeV respectively.

For the linearly polarized photon beam, we will use a 2-mm-diameter collimator. The maximum acceptable rate in the tagger is limited by the rate of a single T-counter and the acceptable accidental rate. Since in this experiment we rely on the missing mass technique, we need good identification of the incident photon. Accidental coincidences lead to particle misidentification. In our estimate,

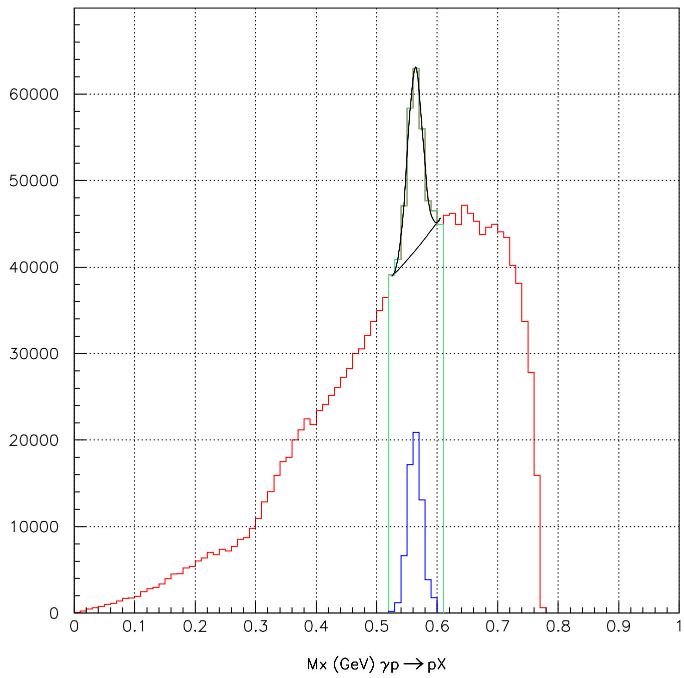

Figure 12: Kinematical cut to select η-production.

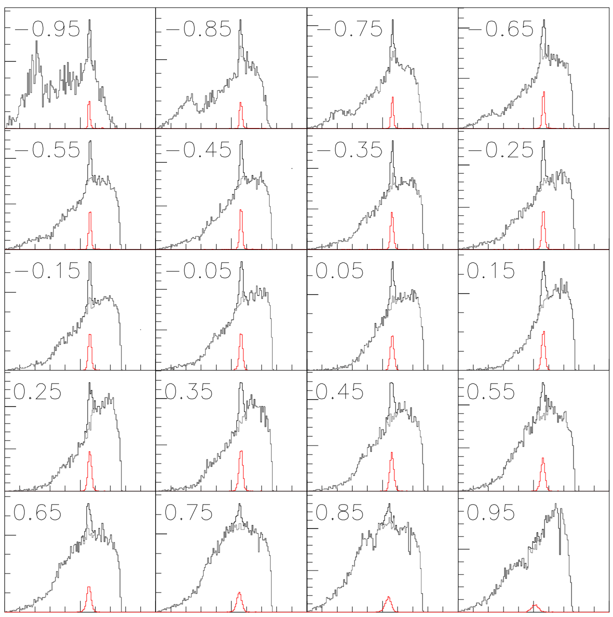

Figure 13: Missing mass spectra for different angular bins.

we used the following numbers: maximum rate per counter 5 MHz, total maximum tagger rate 50 MHz. The acceptable event rate in the DAQ in the previous experiment was about 3.5 kHz. Recent improvements in the CLAS DAQ should permit running at event rates up to 8 kHz.

In case of coherent bremsstrahlung, all the tagger rate is concentrated in a peak about 200 MeV wide that is covered just by only a few T-counters. With all this in mind, we can run with $5 \cdot 10^6 \gamma$/s on target in the range of the coherent peak without overloading the tagger and DAQ, and still have an acceptable rate of the accidental coincidences.

With the lack of previous measurements of asymmetries our goal is to achieve a statistical uncertainty in the polarization observables of 0.1 or less in a reasonable measurement time. To achieve this accuracy we need to collect at least 50K of η-photoproduction events in given photon energy bin. Under described conditions in 50 MeV wide bins in photon energy, we collect about 60K η-photoproduction events detected in CLAS per day at energies below 1.4 GeV, and about half as many for higher energies.

There are several main sources of systematic uncertainties: beam polarization uncertainty, target polarization uncertainty, effective dilution factor uncertainty, instrumental asymmetry in the detector. To minimize effects of the instrumental asymmetry we will flip beam and target polarization. In case of circularly-polarized beam the helicity flips continuously following helicity changes of the electron beam. In case of linearly polarized beam we will rotate polarization plane periodically by changing the orientation of the radiator crystal. Target polarization will be flipped every time we do repolarization. A precise measurement of the target polarization will be done in high filed when target is inside of the polarizing magnet at the beginning and the end of each repolarization cycle. We also will do polarization measurements periodically during an experimental run when the target is in holding field. To get better control of the effective dilution factor we will install additional carbon target and will take data from both targets simultaneously. We use the same estimates for uncertainties as described in approved experiment E02-112 [22]. The estimates are as follows :

- beam polarization 4 – 6%
- target polarization 3 – 4%
- dilution factor 5%.

The observables Σ and T will be extracted from the measurements with two different beam/target polarization. This will be used to evaluate their systematic uncertainties. The relations between various observables described by Equations (12) and (13) of the Appendix is another tool to check for consistency of the data and their systematic uncertainties.

4 Summary and beam time request

We propose to measure with CLAS and the photon tagger in Hall B of Jefferson Lab the observables Σ, T, P, E, F, G, and H in η-photoproduction with a polarized photon beam and polarized frozen spin target for photon energies 0.75 – 2.0 GeV. We will pay a special attention to the range of W 1.5 – 1.8 GeV where there are eight known resonances. We will use finer binning in this range. We will use 25 MeV wide bins in photon energy for energies below 1.4 GeV and 50 MeV wide bins above 1.4 GeV. We will use 10 angular bins within $\cos\theta_{\mathrm{c.m.}}$ range from -0.9 to 0.9. Expected statistical accuracy for all observables is 0.05 – 0.1. This experiment will contribute over 300 data points for each of the seven polarization observables, or over 2000 data points total. Note that the world database currently has a total of 225 data points with polarization.

Table 5: Proposed kinematics in the settings (Set.) A, B, C and D with various beam/target polarizations, collimator diameter (d), proposed running time, incident electron beam energy, covered photon energy range, assumed photon flux on target Φ within the used tagger range (Tgr.).

Set.	#	Beam/Target	d (mm)	Time (h)	E_e (GeV)	E_γ (GeV)		Φ (MHz)	Tgr. (MeV)
A	1	$\uparrow\uparrow$	2.0	48	2.0	0.750	0.900	5.0	200
	2		2.0	48	3.0	0.900	1.050	5.0	200
	3		2.0	96	3.0	1.050	1.200	5.0	200
	4		2.0	96	4.0	1.200	1.350	5.0	200
	5		2.0	96	4.0	1.350	1.500	5.0	200
	6		2.0	96	4.0	1.500	1.650	5.0	200
	7		2.0	96	4.0	1.650	1.800	5.0	200
	8		2.0	96	4.0	1.800	1.950	5.0	200
	9		2.0	96	4.0	1.950	2.000	5.0	200
B	13	$\uparrow\rightarrow$	2.0	24	2.0	0.750	0.900	5.0	200
	14		2.0	36	3.0	0.900	1.050	5.0	200
	15		2.0	36	3.0	1.050	1.200	5.0	200
	16		2.0	48	4.0	1.200	1.350	5.0	200
	17		2.0	48	4.0	1.350	1.500	5.0	200
	18		2.0	48	4.0	1.500	1.650	5.0	200
	19		2.0	48	4.0	1.650	1.800	5.0	200
	20		2.0	72	4.0	1.800	1.950	5.0	200
	22		2.0	72	4.0	1.950	2.000	5.0	200
C	10	$\odot\uparrow$	2.6	100	1.6	0.750	1.500	6.6	full
	11		2.6	140	2.2	1.450	2.000	4.9	full
D	23	$\odot\rightarrow$	2.6	100	1.600	0.750	1.500	5.4	full
	24		2.6	140	2.200	1.450	2.000	8.2	full

The experimental configuration is compatible with three other approved experiments on pion and kaon photoproduction (E02-112, E03-105 and E04-102 [22][23][24]). Proposed beam/target settings are presented in Table 5. The final request coordinated with other already approved experiments is summarized in Table 6. It shows total required time, time that is approved for other experiments that we can use and additional time necessary. The total time required for the proposed program is 70 days of beam on target. About a half of the data for this experiment and the other three approved experiments could be accumulated simultaneously. The time already approved for other experiments that could be used for this experiment is 33 days. The experiment E02-112 has 20 days approved for measurements with linearly polarized beam and transversely polarized target. However, it requires running with two particle trigger most of the time in order to measure triple polarization observables. We cannot collect data for our experiment with this trigger. In this proposal, we request 37 additional days of beam time for production data taking. For settings C and D, high electron beam polarization is required.

Table 6: Summary of beam time request.

Set.	Other expts.	Total time request(days)		
		Total required =	Other expts.	+ This request
A	E02-112	32	5	27
B	E03-105	18	8	10
C	E03-105	10	10	0
D	E04-102	10	10	0
Total		70	33	37

Overheads include the time necessary for target re-polarization, changing the beam energy and polarization orientation. We estimate the total overhead as 10 days.

These measurements will provide an extensive data set with good statistical accuracy and well understood systematic uncertainties. This data will provide stringent tests of models of the nucleon, and provide a definitive data set for nucleon resonance spectrum analyses. The proposed experimental program is a natural continuation of research started in the initial η photoproduction experiment, E91-008 [31]. *Together with experiments E02-112, E03-105 and E04-102, we will mount a package of experiments that will provide essential data of unprecedented quality and kinematical coverage suitable for coupled-channels analysis, one of the milestones in hadronic physics.*

Appendix

The definitions of the variables commonly used to describe meson photoproduction experiments could be found in Refs. [15, 30]. In η photoproduction there could be three polarized objects: photon beam, target and recoil proton. Figure 14 shows the coordinate system we will be using. The frame $\{x, y, z\}$ is related to the target polarization, with the z-axis along the photon momentum $\vec{k}$, the y-axis perpendicular to scattering plane $\vec{y} = \vec{k} \times \vec{q}/\sin\theta$, and x-axis is defined as $\vec{x} = \vec{y} \times \vec{z}$. The frame $\{x', y', z'\}$ is related to the recoil proton polarization, with z'-axis along the η momentum $\vec{q}$, y'-axis is the same as y-axis, and x'-axis is defined as $\vec{x} = \vec{y'} \times \vec{z'}$.

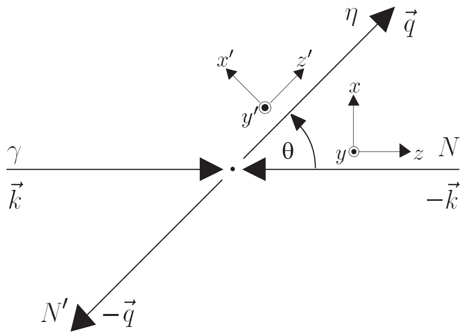

Figure 14: Coordinate systems for polarization vectors in η photoproduction in the c.m. system.

The differential cross sections may be determined by three groups of polarization experiments:

- polarized photons and polarized target (BT)

$$\frac{d\sigma}{d\Omega} = \sigma_0\big[1 - P_T\Sigma\cos 2\varphi + P_x(-P_T H\sin 2\varphi + P_\odot F) - P_y(-T + P_T P\cos 2\varphi) - P_z(-P_T G\sin 2\varphi + P_\odot E)\big]\,, \tag{9}$$

- polarized photons and recoil polarization (BR)

$$\frac{d\sigma}{d\Omega} = \sigma_0\big[1 - P_T\Sigma\cos 2\varphi + P_{x'}(-P_T O_{x'}\sin 2\varphi - P_\odot C_{x'}) - P_{y'}(-P + P_T T\cos 2\varphi) - P_{z'}(P_T O_{z'}\sin 2\varphi + P_\odot C_{z'})\big]\,, \tag{10}$$

- polarized target and recoil polarization (TR)

$$\frac{d\sigma}{d\Omega} = \sigma_0\big[1 + P_{y'}P + P_x(P_{x'}T_{x'} + P_{z'}T_{z'}) + P_y(T + P_{y'}\Sigma) - P_z\,(P_{x'}L_{x'} - P_{z'}L_{z'})\big]\,, \tag{11}$$

where σ_0 denotes the unpolarized differential cross section, P_T the transverse degree of photon polarization, $P_\odot$ the right-handed circular photon polarization, φ the angle between photon polarization vector and reaction plane, and $\vec{P}$ the target polarization. Table 7 summarizes all polarization observables.

These 16 observables are not completely independent. Their relations could be used for the consistency check of the experimental data and for the evaluation of systematic uncertainties.

Table 7: Polarization observables in pseudoscalar meson photoproduction. The entries in parentheses signify that the same polarization observables also appear elsewhere in the table.

Beam	Target				Recoil			Target + Recoil			
	$-$	$-$	$-$	$-$	x'	y'	z'	x'	x'	z'	z'
	$-$	x	y	z	$-$	$-$	$-$	x	z	x	z
unpolarized	σ_0	0	T	0	0	P	0	$T_{x'}$	$-L_{x'}$	$T_{z'}$	$L_{z'}$
linear pol.	$-\Sigma$	H	$(-P)$	$-G$	$O_{x'}$	$(-T)$	$O_{z'}$	$(-L_{z'})$	$(T_{z'})$	$(-L_{x'})$	$(-T_{x'})$
circular pol.	0	F	0	$-E$	$-C_{x'}$	0	$-C_{z'}$	0	0	0	0

Since in this proposal we discuss only the Beam-Target group we present relations only for these observables. There are two relations for this group:

$$E^2 + F^2 + G^2 + H^2 = 1 + P^2 - \Sigma^2 - T^2, \tag{12}$$

and

$$FG - EH = P - \Sigma T. \tag{13}$$

The Equation 9 is a generalized form that describes reaction cross section for any orientation of beam-target polarization. Table 8 contains reduced version of it for particular beam-target combinations. We use following symbols to denote the direction of polarization:

0, $\odot$, $\uparrow$ for unpolarized, circularly polarized, and Linearly polarized photon beam

0, $\rightarrow$, $\uparrow$ for unpolarized, longitudinally polarized and transversely polarized target

Table 8: Cross section for different combinations of beam-target polarizations

Beam	Target	$d\sigma/d\Omega$
0	0	σ_0
0	$\rightarrow$	σ_0
0	$\uparrow$	$\sigma_0\left[1 + P_y T\right]$
$\odot$	0	σ_0
$\odot$	$\rightarrow$	$\sigma_0\left[1 - P_z P_\odot E\right]$
$\odot$	$\uparrow$	$\sigma_0\left[1 + P_x P_\odot F + P_y T\right]$
$\uparrow$	0	$\sigma_0\left[1 - P_T \Sigma \cos 2\varphi\right]$
$\uparrow$	$\rightarrow$	$\sigma_0\left[1 - P_T \Sigma \cos 2\varphi + P_T P_z G \sin 2\varphi\right]$
$\uparrow$	$\uparrow$	$\sigma_0\left[1 - P_T \Sigma \cos 2\varphi - P_x P_T H \sin 2\varphi - P_y(-T + P_T P \cos 2\varphi)\right]$

References

[1] W. -T. Chiang, S. -N. Yang, L. Tiator and D. Drechsel, Nucl. Phys. **A700**, 429 (2002); W. -T. Chiang, private communication.

[2] S. Capstick and W. Roberts, Prog. Part. Nucl. Phys. (Suppl. 2), **45**, S241 (2000).

[3] S. Eidelman *et al.*, *The Review of Particle Physics*, Phys. Lett. B**592**, 1 (2004).

[4] N. C. Mukhopadhay and N. Mathur, Phys. Lett. **B444**, 7 (1998).

[5] L. Tiator, D. Drechsel, and G. Knöchlen, Phys. Rev. C **60**, 035210 (1999).

[6] R. A. Arndt, I. I. Strakovsky, and R. L. Workman, Phys. Rev. C **53**, 430 (1996).

[7] I. G. Aznauryan, *et al.*, nucl-th/0407021 (2004).

[8] B. Krusche, *et al.*, Phys. Rev. Lett. **74**, 3736 (1995).

[9] F. Renard, *et al.*, Phys. Lett. B **528**, 215 (2002).

[10] M. Dugger, *et al.*, Phys. Rev. Lett. **89** 222002 (2002).

[11] V. Crede *et al.*, hep-ex/0311045, (2004).

[12] J. Ajaka *et al.*, Phys. Rev. Lett **81**, 1797 (1998).

[13] A. Bock *et al.*, Phys. Rev. Lett. **81**, 534 (1998).

[14] B. Saghai and Z. Li, Eprint: nucl-th/0202007; B. Saghai, private communication.

[15] I. S. Barker, A. Donnachie, and J. K. Storrow, Nucl. Phys. **B95**, 347 (1975).

[16] W.-T. Chiang and F. Tabakin, Phys. Rev. C **55**, 2054 (1997).

[17] G. Keaton and R. Workman, Phys. Rev. C **53**, 1435 (1996).

[18] R. A. Arndt, I. I. Strakovsky, and R. L. Workman, Phys. Rev. C **62**, 034005 (2000); R. A. Arndt, I. I. Strakovsky, R. L. Workman, and M. M. Pavan, Phys. Rev. C **52**, 2120 (1995); R. A. Arndt, I. I. Strakovsky, and R. L. Workman, in: *Proc. of 9th International Symposium on Meson-Nucleon Physics and the Structure of the Nucleon, Washington, DC, USA, July 26–31, 2001*, Eds. H. Haberzettl and W. J. Briscoe, πN Newslett. **16**, 150 (2002).

[19] B. Mecking *et al.*, Nucl. Instr. Meth. **A 503**, 513 (2003).

[20] D. I. Sober *et al.*, Nucl. Instr. Meth. **A 440**, 263 (2000).

[21] H. Olsen and L. C. Maximon, Phys. Rev. **114**, 887 (1959).

[22] JLab Proposal E02-112, "Search for Missing Nucleon Resonances in the Photoproduction of Hyperons using Polarized Photon Beam and Polarized Target," Spokespersons: F. Klein (contact), L. Todor, and P. Eugenio (2002).

[23] JLab Proposal E03-105, "Pion Production From a Polarized Target," Spokespersons: S. Strauch (contact), N. Benmouna, G. O'Rielly and I. I. Strakovsky (2003).

[24] JLab Proposal E04-102, "Helicity structure of Pion Photoproduction," Spokespersons: D. I. Sober (contact), M. Khandaker and D. G. Crabb (2004).

[25] C. D. Keith *et al.*, Nucl. Instr. Meth. **A 501**, 327 (2003).

[26] O. Dzyubak, C. Djalali and D. Tedeschi, CLAS Note 2004-023 (2004) http://www.jlab.org/Hall-B/notes/clas_notes04/2004-023.pdf

[27] J. H. Billen and L. M. Young, POISSON/SUPERFISH, LANL Report LA-UR-96-1834 (revised April 2003).

[28] OPERA-3D User Guide, VF-01-02-D2 (Vector Fields Ltd., England, 2002).

[29] O. Dzyubak, C. Djalali, N. Recalde and D. Tedeschi, Nucl. Instr. Meth. **A 526**, 132 (2004).

[30] C. G. Fasano, F. Tabakin and B. Saghai, Phys. Rev. C **46** 449 (1992).

[31] TJNAF experiment E91-008, "Photoproduction of η and η' mesons," Spokesperson: B. G. Ritchie (1991).

[32] A. S. Iljinov *et al.*, Nucl. Phys. A **616**, 575 (1997).